Effect of ethanol concentration on methane hydrate decomposition
MD simulation insights

Sun, Xiaoliang; Zhou, Guanggang; Liu, Zilong; Zhu, Jianwei; Guo, Fengzhi; Chen, Junqing; He, Wenhao; Wang, Ning; Zhao, Ge; Lu, Guiwu

DOI
10.1016/j.jmrt.2021.06.004

Publication date
2021

Document Version
Final published version

Published in
Journal of Materials Research and Technology

Available online at www.sciencedirect.com

jmr&t Journal of Materials Research and Technology

journal homepage: www.elsevier.com/locate/jmrt

Original Article

Effect of ethanol concentration on methane hydrate decomposition: MD simulation insights

Xiaoliang Sun [a], Guanggang Zhou [a], Zilong Liu [a,b,**], Jianwei Zhu [a], Fengzhi Guo [a], Junqing Chen [a], Wenhao He [a], Ning Wang [a], Ge Zhao [a], Guiwu Lu [a,*]

[a] Beijing Key Laboratory of Optical Detection Technology for Oil and Gas, College of Science, College of New Energy and Materials, China University of Petroleum (Beijing), Beijing 102249, China

[b] Organic Materials & Interfaces, Department of Chemical Engineering, Faculty of Applied Sciences, Delft University of Technology, Van der Maasweg 9, 2629 HZ Delft, the Netherlands

ARTICLE INFO

Article history:
Received 24 April 2021
Accepted 1 June 2021
Available online 5 June 2021

Keywords:
Methane hydrate
Ethanol concentration
Thermodynamics
Decomposition
Molecular dynamics

ABSTRACT

The controllability of mining is a key factor affecting the commercial application of methane hydrates, and the addition of chemical additives can significantly accelerate the mining process. However, the effect of additive concentration on hydrate decomposition is not yet well understood. In this study, we systematically investigate the effect of ethanol concentration on the decomposition of methane hydrate under varying thermodynamic conditions using molecular dynamics (MD) simulations. To quantitatively characterize the decomposition process and mechanism of methane hydrates, the combination of angular order parameter (AOP), radial distribution function (RDF), mean square displacement (MSD), diffusion coefficients and system energy was for the first time used. The results showed that the addition of ethanol contributed to the formation of methane bubbles and accelerated the decomposition of hydrates. The mass transfer effect of ethanol molecules and the reconstruction of the hydrogen bond network of water molecules determined the stability of hydrates. From 0 to 40 mol% ethanol concentration, the hydrate decomposition increased with increasing the concentration of ethanol. Both increasing the temperature and decreasing the pressure are beneficial to the decomposition of the hydrate system. These results provide the selection of optimal ethanol concentration for the decomposition of methane hydrate and reveal its decomposition mechanism, and shed important light for the controllable production of gas hydrates.

* Corresponding author.
** Corresponding author.
E-mail addresses: zilong@cup.edu.cn (Z. Liu), lugw@cup.edu.cn (G. Lu).

https://doi.org/10.1016/j.jmrt.2021.06.004

1. Introduction

Natural gas hydrate (NGH) is a non-stoichiometric clathrate formed by water molecules (the hosts) and small hydrocarbon molecules (the guests). The water molecules form water cage through hydrogen bonding, and small guest molecules (methane, ethane, hydrogen, carbon dioxide, *etc.*) in the cage combine with water molecules through van der Waals forces, to form the stable inclusion compound under certain thermodynamic conditions. Since NGH looks like ice and can burn, it is also called combustible ice [1]. The configuration of methane hydrate can be divided into three types: style I (sI), style I (sII), and style H (sH). Among them, sI is found to be the most common in naturally occurring hydrates [2].

Methane hydrates exist on the margins of continental plates, and are common on the ocean floor and permafrost, which make the mining process challenging. Methane is also the greenhouse gas, whose greenhouse effect is 21 times higher than that of carbon dioxide. If the mining process is uncontrollable, methane leakage could result in serious environmental problems. Therefore, controllable mining of hydrates is of great importance for practical applications. Common methods of hydrate exploitation mainly include the followings: thermal stimulation method [3,4], depressurization method [3,5], chemical injection method [6–8], gas replacement method [9,10], and the mixture of these methods. Thermal stimulation mining process consumes a large amounts of heat and is economical unfeasible. The depressurization method is easy to cause uncontrollable mining. The gas replacement method has low mining efficiency. Compared with these methods, the chemical injection method has lower energy requirements, higher gas production efficiency, and flexible control of the injection volume. Thus, the chemical injection method has great potential in hydrate mining.

Based on experimental studies, there are various chemical additives assisting the decomposition of hydrates. Daraboina et al. [11] found the use of biological inhibitors of antifreeze proteins not only inhibited the growth of hydrates, but also accelerated the decomposition of hydrates. Pawan et al. [12] investigated the effects of quaternary ammonium salts on the decomposition of natural gas hydrates, and showed that tetramethyl ammonium bromide (TMAB) and tetra-ethyl ammonium bromide (TEAB) showed thermodynamic inhibition, whereas tetra-butyl ammonium bromide (TBAB) showed a promoting effect. Arvind et al. [13] studied the dissociation mechanism of methane hydrate using nuclear magnetic resonance (NMR) method. The experimental results revealed that the occupants of the large and small cages remained unchanged during the hydration decomposition process, indicating no preference for the decomposition of large cages and small cages. The decomposition rates of large and small cages were similar and the whole hydrate cell was decomposed simultaneously. Guembaroski et al. [14] compared the inhibitory effects of ethanol and sodium chloride on carbon dioxide hydrate, and the results demonstrated the better inhibitory effect of sodium chloride than ethanol under high pressure conditions. Meshram et al. [15] reported oxalic acid had a moderate inhibition effect, but succinic acid and aspartic acid had a promotion effect on NGH decomposition.

Nevertheless, there are many limitations in the experimental study of hydrate and it is difficult to observe the kinetic process of hydrate decomposition on the nanoscale, and the operation process is also challenging at low temperature and high pressure conditions. Overcome these issues, molecular dynamics (MD) simulations offer promising route to investigate the hydrate decomposition at nanosecond and nanoscale. Kondori et al. [16] studied the effects of inhibitors on the stability and decomposition of sII hydrate using MD simulations. The simulation results indicated that the order of inhibition performance of different inhibitors was: methanol > ethanol > glycerin. Li et al. [17] adopted the method of MD simulation to analyze the influence of thermodynamic conditions and methane concentration on the decomposition of methane hydrate in water environment, and demonstrated that methane concentration in the surrounding water phase had an inhibitory effect on the decomposition of methane hydrate. Sun et al. [18] studied the effects of methanol and thermodynamic conditions on the decomposition of methane hydrate, and the results showed that methanol could effectively promote the decomposition of methane hydrate. Dai et al. [19] studied the chain length of alcohol, the hydroxyl position and the number of hydroxyl groups on the influence of methane hydrate decomposition using MD simulation, and the results reported that shortening the chain length of alcohol and increasing the alcohol hydroxyl number had promoting effect on methane hydrate decomposition. However, the concentration of alcohols in their simulation was 100 mol%, which was far from the actual situation.

To the best of our knowledge, the effect of chemical additives concentration on hydrate decomposition is not yet well understood. Therefore, we investigated the influence of ethanol concentration and thermodynamic conditions on the decomposition of methane hydrate. By using decomposition snapshot, angular order parameter, radial distribution function, mean square displacement and energy evolution, the micro-evolution process of hydrate decomposition was studied qualitatively and quantitatively. It is expected that this work will provide theoretical guidance for the controllable exploitation of natural gas hydrates assisted by chemical additives.

2. Models and methods

The simulation system in this study is divided into solid and liquid parts. The solid system is the 3×3×3 super cell of sI methane hydrate. The liquid system is ethanol solution, and the total number of molecules in ethanol solution of different concentrations is 200. The size of the whole system is about 3.8×3.8×4.8 nm. Three dimensional periodic boundary conditions are used in the simulation. The construction process of the system is as follows. Firstly, sI hydrate unit cell was constructed according to the data in literature [1], and then the hydrate supercell of 3×3×3 was obtained by cell expansion. Secondly, by using Packmol [20] software, the liquid ethanol solution system was constructed, and the total number of 200 was kept unchanged, so the total liquid system contains X ethanol molecules and (200 - X) water molecules. The final

step is to combine the two systems along the z axis to get the initial configuration of the solid–liquid system. The hydrate system adding 40 mol % ethanol was shown in Fig. 1, and other system of the initial configuration figure were shown in Fig. S1. The water molecule model used in the simulation was TIP4P [21]. The OPLS-UA [22,23] model was adopted for methane molecule and ethanol molecule. These two models have been widely used in hydrate simulation, including the process of hydrate nucleation and decomposition [24,25]. Lorentz–Berthelot mixing rule [26] was adopted for L-J interaction between different molecules, and the parameters were shown in Table 1. The cutoff distances of Coulomb force and L-J interaction were 0.85 nm and 1.20 nm respectively. PPPM algorithm was adopted for long range electrostatic force [27]. Water molecules were constrained by Shake algorithm [28]. Temperature and pressure were maintained by a Nose-Hoover [29–31] thermostat.

LAMMPS [32] was used for all simulations in this work. It is an open source molecular dynamics software with high parallel computing efficiency and can simulate millions of scale systems. It is a widely used simulation software. The simulation process was as follows. Firstly, the oxygen atom of water molecule, methane molecule and liquid layer molecule were fixed, and the system was relaxed with the step length of 2 fs under the ensemble of NVT. The simulation was carried out for 500,000 steps (i.e. 1ns) to obtain a stable hydrate configuration. Secondly, the above fixation operations were cancelled, the hydrate system was fixed, and the liquid layer was simulated with 500,000 steps (i.e. 1ns) under NVT ensemble to obtain a stable liquid layer configuration. Finally,

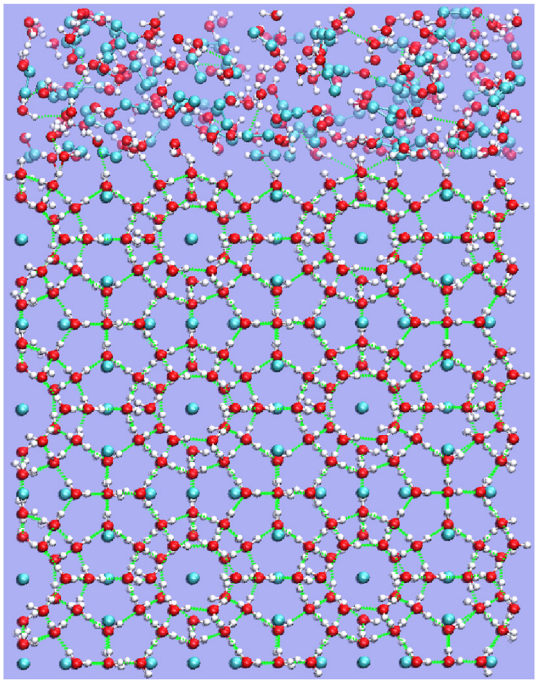

Fig. 1 – Initial configuration diagram. Oxygen, hydrogen, and carbon atoms are represented by red, white, and dark green spheres, respectively, and hydrogen bonds are represented by light green dotted lines. All snapshots in the paper are from VMD [34].

Table 1 – Molecular force field parameters in the simulation system [21–23].

Molecule	Atom	q(e)	σ(Å)	ε(KJ/mol)
H_2O	O	−1.040	3.1536	0.1500
	H	0.520	0.0000	0.0000
CH_4	CH_4	0.000	3.7300	0.2939
CH_3CH_2OH	CH_3	0.265	3.9050	0.1750
	CH_2	0.000	3.9050	0.1180
	O	−0.700	3.0700	0.1700
	H	0.435	0.0000	0.0000

all fixed operations were cancelled, and the whole system was simulated with 5 million steps (i.e. 10 ns) under NPT ensemble. Fig. 2 shows the detailed simulation process. The simulated temperature and pressure conditions were as follows: for the ethanol-hydrate system with different concentrations, the temperature was 277.15 K and the pressure was 200 bar, which were the conditions of the hydrate deposit in the Shenhu area in South China Sea [33]. Then, the simulated temperatures were 267.15–302.15 K and the pressures were 1–200 bar for hydrate adding 40 mol% ethanol.

3. Results and discussion

3.1. *Angular order parameter (AOP)*

The water molecules in hydrate form a relatively stable hydrate cage by hydrogen bond, which can be regarded as a special kind of ice. For the actual ice system, water molecules have a high degree of order. In Ih type ice, there are four oxygen atoms around the oxygen atoms of each water molecule to form 4 coordination with it, and only one hydrogen atom on the O–O atom line. Different states of water molecules have different levels of order. In order to describe the order degree of water molecular system quantitatively, some algorithms or parameters have been developed. Angular order parameter (AOP) is one of them, and its definition is as follows [35]:

$$\mathrm{AOP}_i = \sum_{j=1}^{n_i-1} \sum_{k=j+1}^{n_i} \left(|\cos\varphi_{jik}|\cos\varphi_{jik} + 0.11\right)^2 \quad (1)$$

In the above formula, i, j and k represent the number of oxygen atoms, and ϕ_{jik} is the included angle of j-i-k. The above angles are counted only when the distance between j, k and i is less than 0.35 nm. For water molecular systems of different states, AOP values are different. The AOP for ice is 0, for hydrate is 0.1, and for liquid water is 0.8. The larger value of AOP, the higher disorder of system. The process of hydrate decomposition is the transformation from the solid hydrate with low disorder to the liquid water with high disorder. Therefore, the hydrate decomposition process can be quantitatively determined by counting the AOP of the system at different time.

3.1.1. *The effect of alcohol concentration*

Ethanol, as a commonly used thermodynamic assistant, has been reported to promote hydrate decomposition. However, there is no systematic report on the effect of ethanol solution

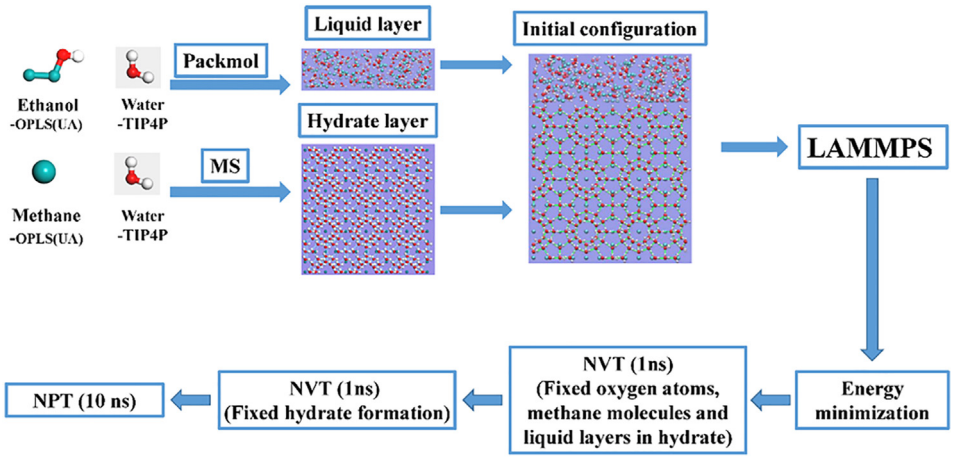

Fig. 2 – Flow chart of modeling and simulation process.

with different concentration on the decomposition of methane hydrate. Fig. 3a shows the variation of AOP with simulation time in the decomposition process of methane hydrate with different concentrations of ethanol solution added. It is obvious that within 0–10 ns, the AOP of 1 mol%, 2 mol% and 5 mol% systems with low concentrations fluctuated within the range of 0.2–0.3, failing to reach 0.8, indicating that these three systems were very stable and did not decompose. AOP of the other systems all reached 0.8 within 10 ns, denoting that the decomposition of the other systems was completed within 10 ns. Decomposition snapshot were displayed in Fig. S2. Fig. 3b shows the time required for AOP of different ethanol concentration systems reaching 0.8. In Fig. 3b, the change of decomposition time with ethanol concentration was not linear, and the hydrate system adding 40 mol% ethanol solution had the minimum value. In order to have a more intuitive understanding of the decomposition rate, the reciprocal of the decomposition time is taken as the relative decomposition rate (RDR) and demonstrated in Fig. S3. It can be seen that the decomposition rate increased firstly and then decreased with the increase of ethanol concentration. The maximum decomposition rate was reached at 40 mol%. This indicates that there is an optimal concentration of ethanol for the decomposition of methane hydrate. It's not that the higher the concentration, the faster the decomposition. This may be due to the fact that there were relatively few ethanol molecules in the low-concentration area, which had less influence on the mass transfer effect of methane molecules. The more ethanol molecules, the more hydrogen bond network of water molecules was destroyed, and the better the effect of promoting hydrate decomposition was. As the concentration increased to a certain value, the mass transfer effect of ethanol molecules on methane molecules gradually increased, and methane molecules could not rapidly diffuse out of the solid–liquid interface, leading to methane molecules gathering near the hydrate, increasing the concentration of methane molecules and decreasing the decomposition driving force. Fig. 4 shows a snapshot of hydrate adding 40 mol % ethanol solution. It is obvious that with the increase of simulation time, the hydrate decomposed layer by layer from 0 to 2 ns, small bubbles appeared at 4ns, bubbles grew larger at 4–6 ns, bubbles further grew larger at 6–7 ns, bubbles disappeared at 7–7.2 ns, forming a stable gas–liquid interface, and the gas–liquid system was stable at 7.2–10ns. The presence of bubbles accelerated the decomposition of hydrates, and similar bubbles appeared in other systems. The formation of bubbles was because that with the decomposition of hydrate, methane molecules in the hydrate entered into the

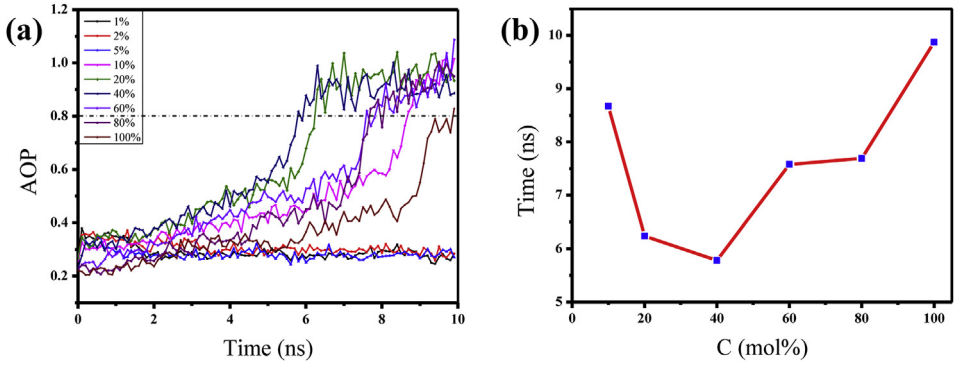

Fig. 3 – (a) AOP of hydrate system with different concentrations of ethanol solution added changing with simulation time, and (b) the time required for AOP to reach 0.8.

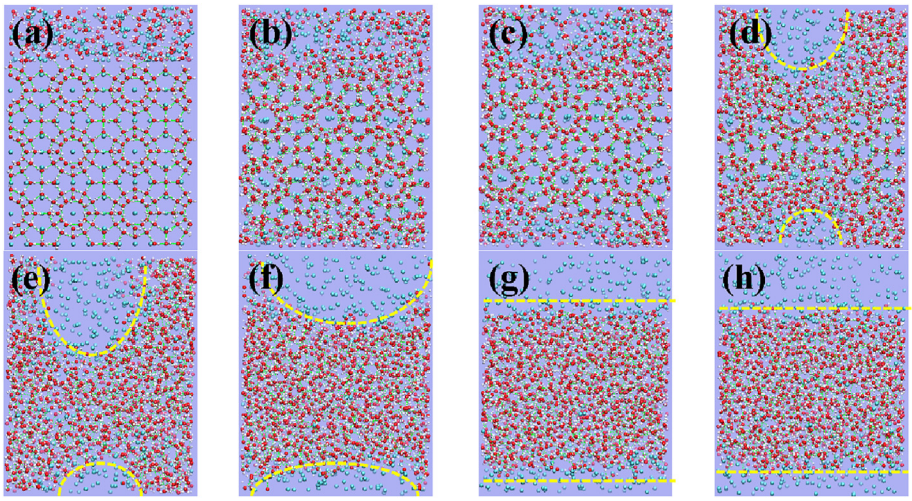

Fig. 4 – Snapshot of hydrate at different moments when adding 40 mol% ethanol solution. (a) 0 ns; (b) 1 ns; (c) 2 ns; (d) 4 ns; (e) 6 ns; (f) 7 ns; 7.2 ns (g); (h) 10 ns.

alcohol solution. Because the solubility of methane molecules was limited, when the methane molecules cannot be dissolved, methane bubbles would be formed. With the increase of the bubble, methane concentration in the liquid phase was reduced, methane concentration near methane hydrate is reduced, diffusion of the methane hydrate to liquid phase increased the driving force, which was advantageous to the hydrate decomposition. This phenomenon was also evident in other work [25].

3.1.2. *The effect of temperature*

The temperature and pressure simulated above was 277.15 K and 200 bar, which was the temperature and pressure condition of hydrate deposit in Shenhu area of South China Sea. In fact, hydrates absorb heat as they decompose, and if there is no an external source of heat, the hydrate temperature will decrease as the decomposition proceeds. Therefore, it is of practical significance to study the decomposition process of hydrate system after adding ethanol at different temperatures. The results in Fig. 3 evince that ethanol solution with the concentration of 40 mol% has the greatest influence on the decomposition of methane hydrate. Here, methane hydrate with a concentration of 40 mol% ethanol solution was selected as the initial configuration to study the rule of the solid–liquid system changing with the temperature at 267.15–302.15 K and the pressure at 200 bar. The variation of AOP at different temperatures with simulation time was available in Fig. 5a. It indicated that AOP of 267.15 K and 272.15 K fluctuated in the range of 0.1–0.4, but failed to reach 0.8, indicating that hydrate systems of these two low temperature systems were stable in the simulation process until 10 ns. Fig. 5b proved the time required for AOP of each system to reach 0.8. As the temperature increased, the time required for AOP of each system to reach 0.8 decreased gradually. Fig. S4 presented the variation trend of relative decomposition rate with the rise of decomposition temperature. It manifested that, with the rise of temperature, the decomposition rate of ethanol-hydrate system was faster, which is consistent with the Dai's work [19].

3.1.3. *The effect of pressure*

In the process of hydrate mining, the depressurization method is a common method, but there are some problems in the depressurization method. The pressure is hard to control in the mining process, and is prone to cause accidents. Hence,

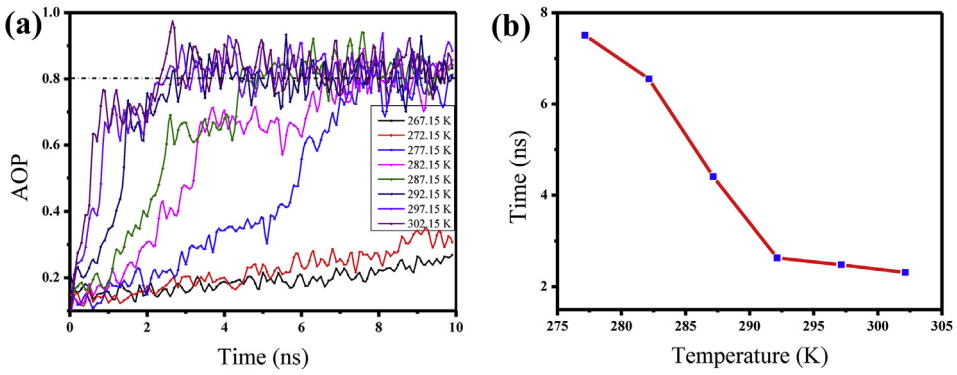

Fig. 5 – (a) AOP changes over simulation time and (b) the time required for AOP to reach 0.8 of hydrate system adding 40 mol % ethanol solution with different temperatures.

a controllable mining method is required. Adding chemical additives is a relatively stable and reliable method. It is of practical significance to study the effects of different chemical additives on the decomposition of methane hydrate. The actual mining process is often the simultaneous use of multiple mining methods. It is of practical significance to study the decomposition process of methane hydrate system with the addition of ethanol solution under different pressures. Here, the 40 mol% concentration of ethanol-hydrate system was selected as the initial configuration, the pressure was 1–200 bar, and the temperature was constant at 277.15 K. Fig. 6a revealed that under the condition of 1–200 bar, the AOP of methane hydrate with 40 mol% ethanol solution reached 0.8 within 10 ns, indicating that each system had completed decomposed.

Fig. 6b made clear that with the increase of pressure, the time required for system AOP to reach 0.8 gradually increased. Fig. S5 displayed that RDR decreased with the increase of pressure, indicating that the decomposition rate of ethanol-hydrate system decreased with the increase of pressure. However, the influence of pressure on the decomposition of hydrate system didn't change linearly. In the low pressure zone (1–10 bar), the RDR slope was -5.97×10^{-3}. In the high pressure area (10–200 bar), the RDR slope was -1.94×10^{-4}, which is about 3% of the RDR slope in the low pressure area. This indicated that the influence of pressure on hydrate decomposition was decreasing in the high pressure area. This may be due to the solubility of methane increases with the increase of pressure at high pressure, which leads to the increase of methane concentration around the hydrate and the decrease of hydrate decomposition rate. In the process of depressurization combined with the addition of ethanol, the appropriate concentration and pressure of ethanol can be selected to achieve controllable exploitation of hydrate.

3.2. *Radial distribution function (RDF)*

The radial distribution function (RDF) is used to evaluate the distribution probabilities of other particles around a given particle in space. Some structural parameters of the substance can be quantitatively evaluated by analyzing RDF. For the hydrate system, the first peak of RDF between carbon atoms of methane molecules represents the average distance between carbon atoms in different cages. The first peak of RDF between oxygen atoms of water molecule represents the distance between adjacent oxygen atoms in water molecule, as shown in Fig. 7a. The second peak of RDF between oxygen atoms represents the crystal structure parameters of sI hydrates with tetrahedral hydrogen bond network.

3.2.1. *The effect of alcohol concentration*

Fig. 7a showed the RDF between oxygen atoms of water molecules at 6 ns in methane hydrate system with different concentrations of ethanol solution added. The first peak

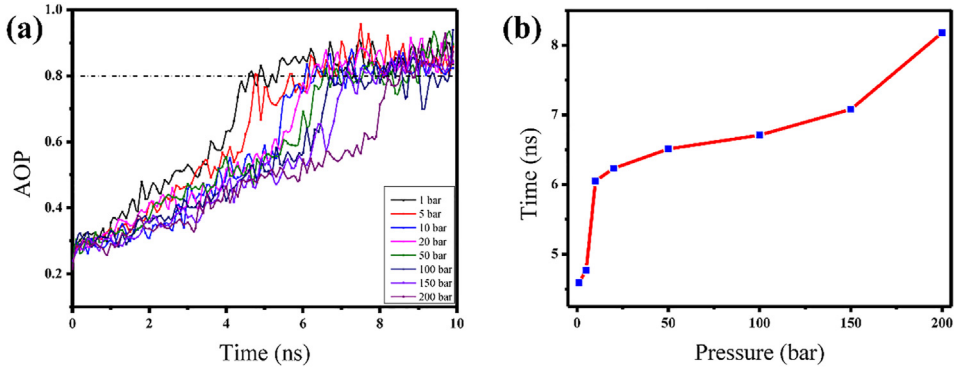

Fig. 6 – (a) AOP changes over simulation time and (b) the time required for AOP to reach 0.8 of hydrate system adding 40 mol % ethanol solution with different pressures.

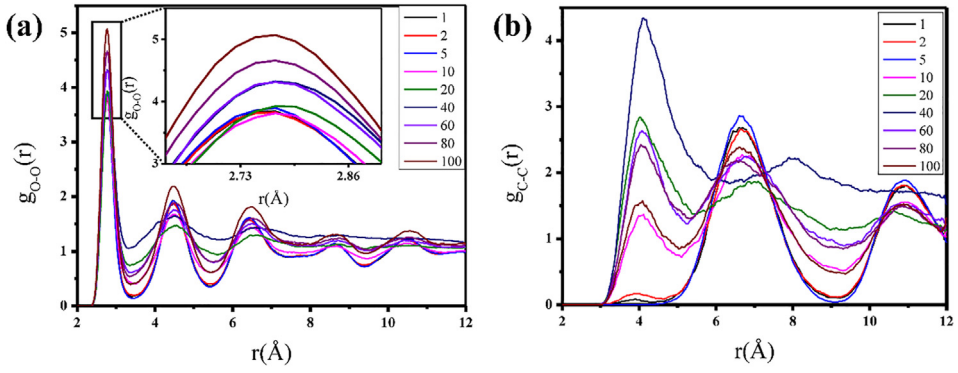

Fig. 7 – The RDF of (a)oxygen atoms in water molecules and (b)carbon atoms in methane molecules within hydrate system adding different concentrations of ethanol at 277.15 K and 200 bar.

emerged at 2.75 Å, which was the distance between the oxygen atoms of the water molecules that form hydrogen bonds. When the concentration was greater than 40 mol%, the first peak rose rapidly, indicating that the higher the concentration of ethanol is, the more stable the methane hydrate is and the slower the decomposition rate is. This was consistent with the results in Fig. 3. When the concentration was greater than 40 mol%, the RDF of hydrate decreased gradually and the decomposition rate slows down. Fig. 7b made clear the RDF of methane molecules in methane hydrate with different concentrations of ethanol at 6 ns. The first peak was the highest at 40 mol%, denoting that the hydrate system with lower and higher concentration of ethanol solution is relatively stable, and methane hydrate is difficult to decompose. At low concentration (<40 mol%), the ability of methanol to break hydrogen bonds between water molecules increased with the increase of methanol concentration, and the decomposition rate was positively correlated with the concentration of ethanol. However, at higher concentrations (>40 mol%), methane molecules were affected by the mass transfer effect in the system. With the increase of ethanol concentration, it became more difficult for methane molecules to pass through the ethanol solution, and the diffusion efficiency of methane from hydrate to solution decreased. Methane molecules were concentrated near the hydrate, which caused the decomposition rate of methane hydrate to decrease.

3.2.2. *The effect of temperature*

Fig. 8a demonstrated the O–O RDF of water molecules at different temperatures in the methane hydrate system with 40 mol% ethanol solution. The first peak decreased with increasing temperature, indicating that the stability of hydrate decreased with increasing temperature. The second peak and the third peak also decreased with the increase of temperature, indicating that the hydrate clathrate was destroyed, and the disorder degree of water molecules in the hydrate increased, from a remote ordered solid state to a disordered liquid state. Fig. 8b presented the C–C RDF of the methane molecule. The first peak increased rapidly with increasing temperature, denoting that the higher the temperature, the greater the probability that methane molecules would form methane clusters after they escape from the cage, and the easier it is for the hydrate to decompose. The second peak appeared at 6.61 Å, which was the distance between methane molecules in the hydrate cage, meaning that the closest distance between methane molecules in the hydrate structure was 6.61 Å. As the temperature increased, the second peak decreased significantly, indicating that methane molecules escaped from the hydrate cage. The escaped methane molecules gathered at 4.10 Å and formed a new peak. As the temperature increases, the first peak increased, indicating that the degree of hydrate decomposition became greater.

3.3. *Mean square displacement (MSD)*

The mean square displacement is used to evaluate the diffusion behavior of particles, and its definition formula is as follows:

$$MSD = \left(\left| \vec{r}_i - \vec{r}_{i0} \right|^2 \right) = \frac{1}{N} \sum_{i=1}^{N} \left(\left| \vec{R}_i(t) - \vec{R}_{i0}(t) \right|^2 \right) \quad (2)$$

in which, N represents the total number of particles, $\vec{R}_i(t)$ is the position of particle i at the time t, and $\vec{R}_{i0}(t)$ represents the position of particle i at the initial moment. Through the MSD, the diffusion coefficient can be obtained by using the Einstein relation [36], which as follows:

$$6D \cdot t = MSD \quad (3)$$

where D indicates the diffusion coefficient, t represents the time, and MSD is the mean square displacement.

3.3.1. *Concentration effect*

Fig. 9a made clear the MSD of methane molecules in the methane hydrate system with different concentrations of ethanol solution. As the simulation time increased, MSD first rose slowly, then rose quickly. This was due to the methane molecules were trapped in the hydrate cage at the beginning of the simulation, so the MSD value was very small. With the decomposition of methane hydrate, methane molecules escaped from the hydrate cage, and the MSD value of methane rose rapidly. The MSD of the 40 mol% system before 6 ns was the highest. In Fig. 9b, it was clear that the diffusion coefficient of the 40 mol% system before 6 ns was the largest, indicating that the 40 mol% system had the fastest decomposition rate.

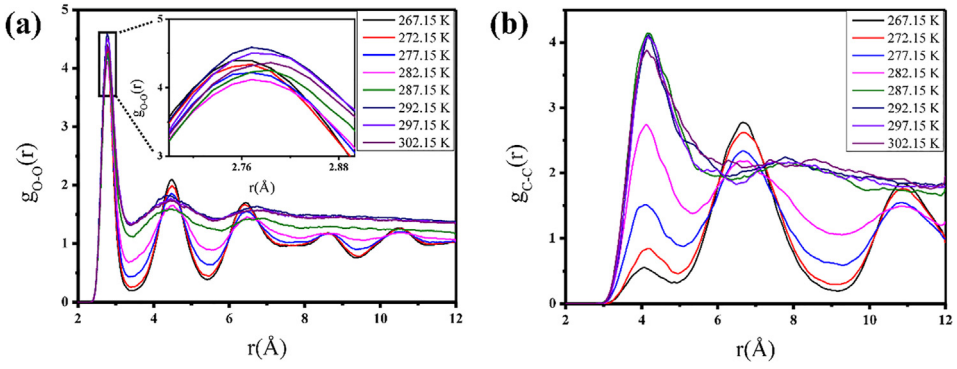

Fig. 8 – The RDF of (a) oxygen atoms in water molecules and (b) carbon atoms in methane molecules at 3 ns under different temperatures in hydrate system with addition of 40 mol% ethanol solution.

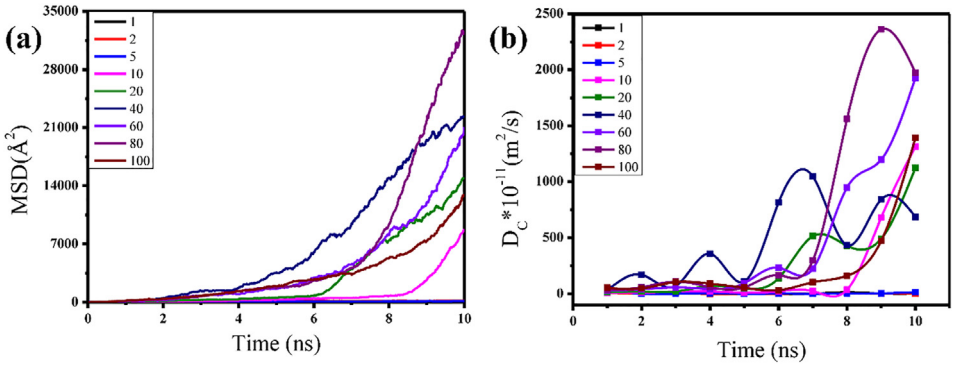

Fig. 9 – (a) MSD and (b) diffusion coefficient of methane molecules in hydrates with different concentrations of ethanol solution added.

This was consistent with the conclusion obtained in Fig. 3. The 40 mol% ethanol solution had the greatest impact on the decomposition of hydrates. This is the result of the comprehensive effect of alcohol molecules breaking the hydrogen bonds of water molecules and affecting the mass transfer effect of methane molecules.

3.3.2. *The effect of temperature*

Fig. 10a displayed the MSD of methane molecules within 0–10 ns in a methane hydrate system with 40 mol% ethanol at 267.15–302.15 K and 200 bar. The MSDs of 267.15 K and 272.15 K were almost unchanged, indicating that the methane molecules at these two temperatures were trapped in the hydrate cage and the hydrate was stable, which was consistent with the conclusion of Fig. 4. The MSD of other systems rose slowly and then rose quickly with the increase of simulation time, indicating that the methane molecules gradually changed from the confined state in the water molecule cage to the free state. As the temperature increased, the MSD increased at the same time, denoting that the higher the temperature, the easier it is for methane molecules to escape from the hydrate cage, the faster the decomposition rate, and the rapid increase in methane MSD value. It was clear from Fig. 10b that the diffusion coefficients of the two systems of 267.15 K and 272.15 K were very low, indicating that the two systems were stable. The diffusion coefficients of other systems gradually increased with the increase of simulated temperature. The results revealed that as the temperature increases, methane molecules were more likely to escape from the hydrate cage, and methane hydrates were easier to decompose. This was consistent with the conclusion in Fig. 4, the higher the temperature, the faster the decomposition of methane hydrate.

3.4. *Total energy*

The decomposition of methane hydrate can actually be regarded as the process of transforming from the solid phase to the liquid phase. The decomposition process needs to absorb energy, so the decomposition of methane hydrate is endothermic, and the total energy of the system increases with the decomposition. When methane hydrate is completely decomposed, the total potential energy of the system tends to stabilize with the increase of simulation time. The speed of decomposition can be evaluated by tracking the energy of the system over time. Fig. 11a presented the curve of the total energy of the hydrate system with different concentrations of ethanol solution as simulation time rose. It was obvious that the energy of the 40 mol% system first reached the maximum value, and then fluctuated near the maximum value due to thermodynamic fluctuations, which was consistent with the conclusion obtained in Fig. 3. The 40 mol% ethanol solution had the best effect on promoting the decomposition of hydrate. Fig. 11b displayed the energy curve of the system with 40 mol% ethanol solution hydrate added under different temperature conditions. It was obvious that as

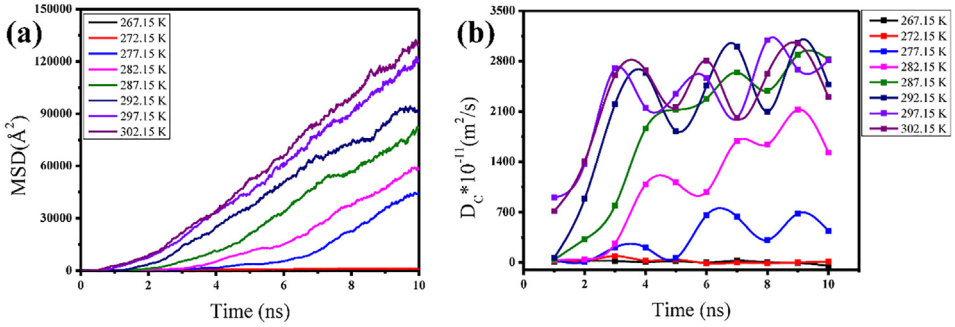

Fig. 10 – (a) MSD, (b) diffusion coefficient of methane molecules in hydrate with 40 mol% ethanol solution at different temperatures.

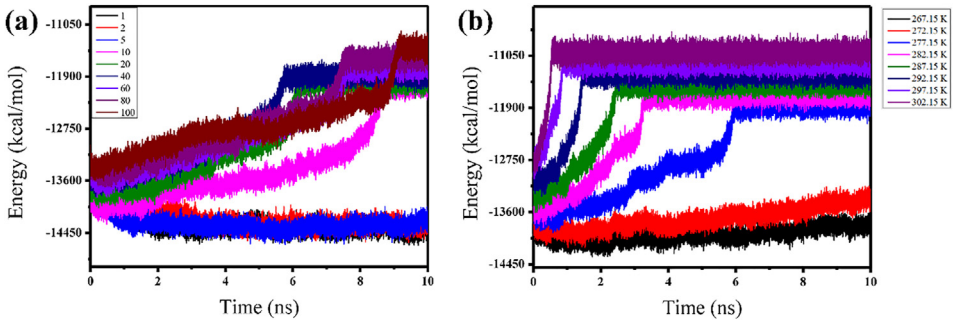

Fig. 11 – (a) Energy curves of methane hydrate system with different concentrations of ethanol solution added, and (b) energy curves of methane hydrate system with 40 mol% ethanol added at different temperatures.

the temperature increased, the time for the system energy to reach the maximum became shorter, indicating that the higher the temperature, the faster the decomposition of the system will be, which was consistent with the conclusion obtained in Fig. 4. The higher the temperature, the higher the kinetic energy of the methane molecules, the easier it is to break through the water cage, making the hydrate easier to decompose.

4. Conclusions

To reveal the decomposition mechanism of ethanol concentration on methane hydrate, we systematically investigated the decomposition process of hydrate by combining four important parameters of AOP, RDF, MSD and total energy using MD simulations. It offers a new route to quantitatively determine the decomposition phenomenon under different alcohol concentrations, temperature and pressure conditions. Based on AOP, RDF, MSD and energy analysis, it was found that the 40 mol% ethanol solution had the most promoting effect on the decomposition of methane hydrate, indicating an optimal concentration for the hydrate decomposition. In the range of 0–40 mol% ethanol concentration, the hydrate decomposition became faster with increasing the ethanol concentration. When the concentration exceeded 40 mol%, the mass transfer effect was significantly improved and limited the diffusion of methane molecules, leading to the accumulation of methane molecules near the hydrate, which made the methane in the hydrate difficult to diffuse to the liquid phase and slowed the decomposition. At the same time, the formation of methane bubbles contributed to the decomposition of methane hydrate. This is owing to that the formation of bubbles reduces the concentration of methane in the liquid phase and facilitates the diffusion of methane around the hydrate to the liquid phase.

Increasing the temperature is conducive to the decomposition of methane hydrate. The higher the temperature, the higher the kinetic energy of methane molecules. Thus, the more unstable the hydrate cage, and the easier the decomposition of the hydrate. Increasing the pressure will inhibit the decomposition of hydrate, the lower the pressure, the faster the decomposition of hydrate. The obtained results quantitatively characterized the decomposition mechanism of methane hydrates, providing new insights into controllable exploitation of hydrates, as well as promoting the efficient application of alcohols and other additives in hydrate development.

Declaration of Competing Interest

The authors declare that they have no known competing financial interests or personal relationships that could have appeared to influence the work reported in this paper.

Acknowledgements

The authors thank Prof. Ernst J.R. Sudhölter of TU Delft for his active discussions and valuable suggestions. The computations were performed on LAMMPS at Shenzhen Supercomputing Center. This work was supported by the Science Foundation of China University of Petroleum, Beijing (No. 2462020BJRC007, 2462020YXZZ003).

Appendix A. Supplementary data

Supplementary data to this article can be found online at https://doi.org/10.1016/j.jmrt.2021.06.004.

REFERENCES

[1] Sloan ED, Koh C. Clathrate hydrates of natural gases. 3rd ed. Boca Raton,FL: CRC Press; 2008.
[2] Buffett BA. Clathrate hydrates. Annu Rev Earth Planet Sci 2000;28(1):477–507.
[3] Wang Y, Feng J-C, Li X-S, Zhan L, Li X-Y. Pilot-scale experimental evaluation of gas recovery from methane hydrate using cycling-depressurization scheme. Energy 2018;160:835–44.
[4] Feng J-C, Wang Y, Li X-S. Dissociation characteristics of water-saturated methane hydrate induced by huff and puff method. Appl Energy 2018;211:1171–8.
[5] Zhan L, Wang Y, Li X-S. Experimental study on characteristics of methane hydrate formation and dissociation in porous medium with different particle sizes using depressurization. Fuel 2018;230:37–44.
[6] Li Z, Jiang F, Qin H, Liu B, Sun C, Chen G. Molecular dynamics method to simulate the process of hydrate growth in the presence/absence of khis. Chem Eng Sci 2017;164:307–12.

[7] Li M, Dong S, Li B, Liu C. Effects of a naturally derived surfactant on hydrate anti-agglomeration using micromechanical force measurement. J Ind Eng Chem 2018;67:140–7.
[8] Feng J-C, Wang Y, Li X-S. Hydrate dissociation induced by depressurization in conjunction with warm brine stimulation in cubic hydrate simulator with silica sand. Appl Energy 2016;174:181–91.
[9] Stanwix PL, Rathnayake NM, de Obanos FPP, Johns ML, Aman ZM, May EF. Characterising thermally controlled Ch4–Co2 hydrate exchange in unconsolidated sediments. Energy Environ Sci 2018;11(7):1828–40.
[10] Xu C-G, Cai J, Yu Y-S, Yan K-F, Li X-S. Effect of pressure on methane recovery from natural gas hydrates by methane-carbon dioxide replacement. Appl Energy 2018;217:527–36.
[11] Daraboina N, Linga P, Ripmeester J, Walker VK, Englezos P. Natural gas hydrate formation and decomposition in the presence of kinetic inhibitors. 2. Stirred reactor experiments. Energy Fuel 2011;25(10):4384–91.
[12] Gupta P, Chandrasekharan Nair V, Sangwai JS. Phase equilibrium of methane hydrate in the presence of aqueous solutions of quaternary ammonium salts. J Chem Eng Data 2018;63(7):2410–9.
[13] Gupta A, Dec SF, Koh CA, Sloan ED. Nmr investigation of methane hydrate dissociation. J Phys Chem C 2007;111(5):2341–6.
[14] Guembaroski AZ, Marcelino Neto MA, Bertoldi D, Morales REM, Sum AK. Phase behavior of carbon dioxide hydrates: a comparison of inhibition between sodium chloride and ethanol. J Chem Eng Data 2017;62(10):3445–51.
[15] Meshram SB, Kushwaha OS, Reddy PR, Bhattacharjee G, Kumar R. Investigation on the effect of oxalic acid, succinic acid and aspartic acid on the gas hydrate formation kinetics. Chin J Chem Eng 2019;27(9):2148–56.
[16] Kondori J, Zendehboudi S, James L. Molecular dynamic simulations to evaluate dissociation of hydrate structure ii in the presence of inhibitors: a mechanistic study. Chem Eng Res Des 2019;149:81–94.
[17] Li K, Chen B, Song Y, Yang M. Molecular dynamics simulation of the effects of different thermodynamic parameters on methane hydrate dissociation: an analysis of temperature, pressure and gas concentrations. Fluid Phase Equil 2020;516:112606.
[18] Sun X, Zhou G, Zhu J, Wu H, Lu G, Bai D. Molecular dynamics simulation of methane hydrate decomposition in the presence of alcohol additives. ChemPhysChem 2019;20(19):2553–65.
[19] Dai C, Hu Y, Wu Y, Zhao M, Yue T. Effects of structural properties of alcohol molecules on decomposition of natural gas hydrates: a molecular dynamics study. Fuel 2020;268:117322.
[20] Martínez L, Andrade RA, Birgin EG, Martínez J. Packmol: a package for building initial configurations for molecular dynamics simulations. J Comput Chem 2010;30(13):2157–64.
[21] Jorgensen WL, Chandrasekhar J, Madura JD, Impey RW, Klein ML. Comparison of simple potential functions for simulating liquid water. J Chem Phys 1983;79(2):926–35.
[22] Jorgensen WL, Madura JD, Swenson CJ. Optimized intermolecular potential functions for liquid hydrocarbons. J Am Chem Soc 1984;106(22):6638–46.
[23] Jorgensen WL. Optimized intermolecular potential functions for liquid alcohols. J Phys Chem 1986;90(7):1276–84.
[24] Yagasaki T, Matsumoto M, Tanaka H. Adsorption mechanism of inhibitor and guest molecules on the surface of gas hydrates. J Am Chem Soc 2015;137(37):12079–85.
[25] Yagasaki T, Matsumoto M, Andoh Y, Okazaki S, Tanaka H. Effect of bubble formation on the dissociation of methane hydrate in water: a molecular dynamics study. J Phys Chem B 2014;118(7):1900–6.
[26] Bernal JD, Fowler RH. A theory of water and ionic solution, with particular reference to hydrogen and hydroxyl ions. J Chem Phys 1933;1(8):515–48.
[27] Hockney RW, Eastwood JW. Computer simulation using particles. Taylor & Francis, Inc.; 1988.
[28] Ryckaert JP, Ciccotti G, Berendsen HJC. Numerical integration of the cartesian equations of motion of a system with constraints: molecular dynamics of N -alkanes. J Comput Phys 1977;23(3):327–41.
[29] Hoover WG. Canonical dynamics: equilibrium phase-space distributions. Phys Rev 1985;31(3):1695–7.
[30] Hoover WG. Constant-pressure equations of motion. Phys Rev 1986;34(3):2499–500.
[31] Melchionna S, Ciccotti G, Holian BL. Hoover npt dynamics for systems varying in shape and size. Mol Phys 1993;78:533–44.
[32] Plimpton S. Fast parallel algorithms for short-range molecular dynamics. J Comput Phys 1995;117:1–19.
[33] Qin X, Liang Q, Ye J, Yang L, Qiu H, Xie W, et al. The response of temperature and pressure of hydrate reservoirs in the first gas hydrate production test in South China Sea. Appl Energy 2020;278:115649.
[34] Humphrey W, Dalke A, Schulten K. Vmd: visual molecular dynamics. J Mol Graph 1996;14(1):33–8.
[35] Bez Luis; A, Clancy Paulette. Computer simulation of the crystal growth and dissolution of natural gas hydrates. Ann N Y Acad Sci 1994;715(1):177–86.
[36] Allen MP, Tildesley DJ, Banavar JR. Computer simulation of liquids. Phys Today 1989;42(3):105–6.